

## Failure analysis of a transmission tower during a microburst

A. Y. Shehata\*

*Atomic Energy of Canada Limited, Mississauga, Ontario, Canada*

A. A. El Damatty‡

*Department of Civil and Environmental Engineering,  
The University of Western Ontario, London, Ontario, Canada*

*(Received October 15, 2007, Accepted April 10, 2008)*

**Abstract.** This paper focuses on assessing the failure of one of the transmission towers that collapsed in Winnipeg, Canada, as a result of a microburst event. The study is conducted using a fluid-structure numerical model that was developed in-house. A major challenge in microburst-related problems is that the forces acting on a structure vary with the microburst parameters including the descending jet velocity, the diameter of the event and the relative location between the structure and the jet. The numerical model, which combines wind field data for microbursts together with a non-linear finite element formulation, is capable of predicting the progressive failure of a tower that initiates after one of its member reaches its capacity. The model is employed first to determine the microburst parameters that are likely to initiate failure of a number of critical members of the tower. Progressive failure analysis of the tower is then conducted by applying the loads associated with those critical configurations. The analysis predicts a collapse of the conductors cross-arm under a microburst reference velocity that is almost equal to the corresponding value for normal wind load that was used in the design of the structure. A similarity between the predicted modes of failure and the post event field observations was shown.

**Keywords:** downburst; microburst; finite element; transmission tower; transmission line; failure; wind.

---

### 1. Introduction

Assessment of the failure incidents of transmission line structures emphasized the importance of taking into account localized high intensity wind events, such as microbursts, in designing this type of structures. Transmission line failures due to high intensity wind have become a dominant threat and a costly problem in the Americas, Australia, South Africa and many other countries around the world (Savory, *et al.* 2001). The failure of a transmission line is usually accompanied with a disruption of electrical services that causes disturbing negative social and economical consequences. For example, in 1996, Manitoba Hydro, Canada, reported a failure of nearly 19 transmission towers

---

\* Structural Engineer, E-mail: [shehataa@aecl.ca](mailto:shehataa@aecl.ca)

‡ Professor, Corresponding Author, E-mail: [damatty@uwo.ca](mailto:damatty@uwo.ca)

during a microburst event (McCarthy and Melsness 1996). This wind damage costed the company about 10 million dollars in losses and caused an interruption in the electrical services that lasted for about five days (Bipole 1 & 2 HVDC transmission line failure report 1999).

This study is a part of an extensive research program initiated by Manitoba Hydro and other major utility companies in Canada to investigate the behaviour of transmission lines under microburst loading. The objective is to improve the current practice applied in the design of transmission towers by accounting for the effect of high intensity localized wind load events. The current study focuses on studying the failure mechanism of one of the typical towers that failed during the 1996 Manitoba microburst event.

Although it has been well reported that microburst events cause frequent failures of transmission line structures, very little attempts were done to study in depth those failures. Savory, *et al.* (2001) conducted a research study on a latticed transmission tower under microburst wind loading. In this study, the behaviour of the tower was investigated under specific microburst parameters. The microburst loading acting on the conductors and the ground wire cables were not considered in this study. Also, only the radial component of the microburst wind speed was considered. The predicted failure mode of the transmission tower showed that the horizontal shear force was the main reason for the collapse of the tower.

A fluid-structure numerical model was previously developed by Shehata, *et al.* (2005) specifically for the microburst analysis of transmission line structures. One of the challenges of microburst-related structural problems is that the acting forces vary with the characteristics of the microburst, such as its diameter and its descending velocity as well as the relative distance between the event and the structure. This numerical model is extended in the current study to investigate the progressive failure of transmission towers under microburst loading. The study starts by determining the critical microburst parameters and the associated velocity fields that are likely to lead to a state of instability of the tower members. The wind loads resulting from those fields are incrementally increased by gradually upgrading the value of the microburst jet velocity till one of the tower members reaches its ultimate capacity. The values of the critical jet velocities at which an onset of buckling occurs for members located at various regions of the tower are reported. For a number of critical cases, progressive failure analyses are carried out by conducting numerical iterations during which various members progressively fail till the structure loses its overall stability.

## 2. Description of the modelled transmission line

A Manitoba Hydro transmission line located in Winnipeg, Manitoba, Canada is considered in the study. In 1996, this transmission line suffered from a failure of about 19 transmission towers during a microburst event (McCarthy and Melsness 1996). One of the failed towers was chosen in the current study to illustrate and assess the failure mechanism of transmission towers under such a type of localized wind loading. The tower is labelled as Type A-402-0 guyed tower (Manitoba Hydro 1991). Fig. 1 shows the geometry of the modeled tower. It is categorized as a guyed tower since it is supported by a pin at the base and by four supporting guys at an elevation of 35.18 (m) relative to the ground. The total height of the tower is 44.39 (m) and the conductors are attached to the tower through insulator strings at a height of 38.23 (m).

## 3. Fluid-structure numerical model

A brief description of the numerical model employed in the current study is provided in this

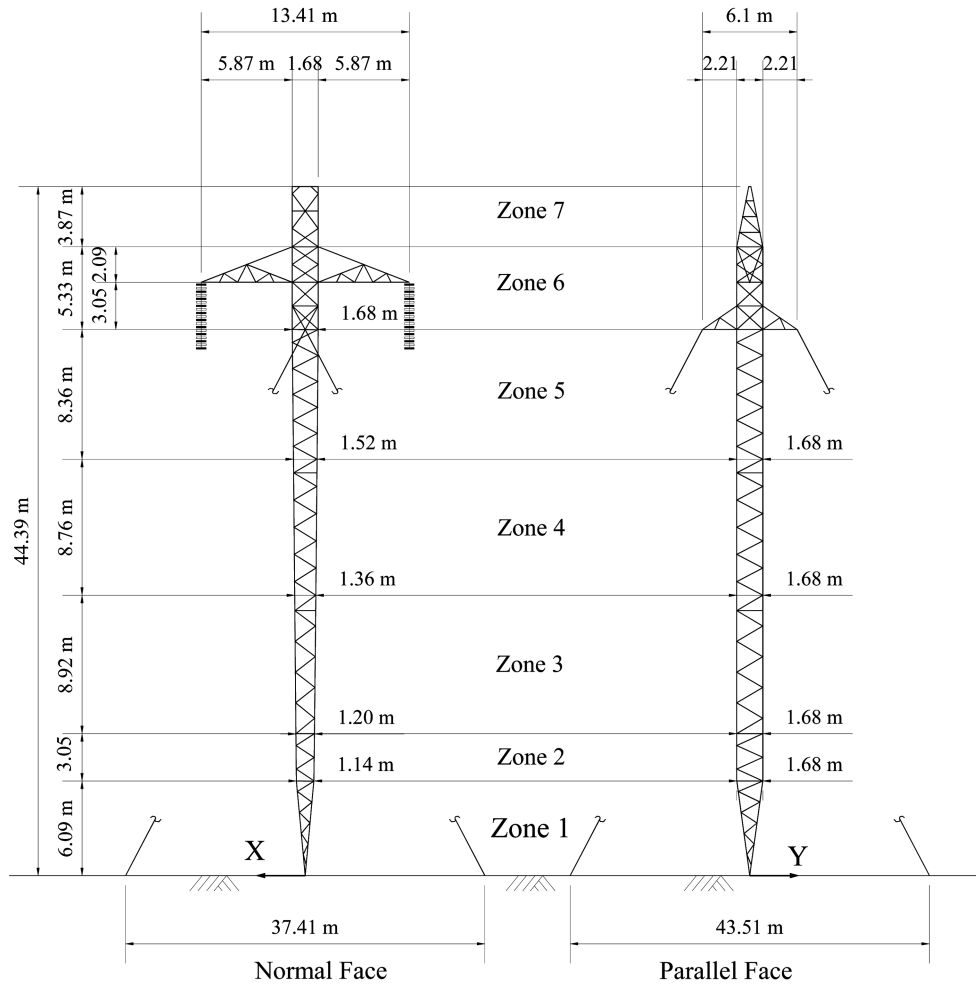


Fig. 1 Geometry of the modelled lattice transmission tower

section. For more details, the reader is referred to the study conducted by Shehata, *et al.* (2005). Various steps applied in this numerical model are illustrated through the flow chart diagram provided in Fig. 2 and are briefly described below.

### 3.1. Modelling of a transmission line

The tower members and the guys are modelled using three-dimensional linear frame elements having two nodes and six degrees of freedom per node; three translational and three rotational. The conductors and ground wire cables are modelled using a two-dimensional curved beam element (Koziey and Mirza 1994, Gerges and El Damatty 2002) that takes into account the non-linear behaviour associated with the large deformation experienced by these cables. Two separate sets of analyses are conducted for the cables to determine their responses to the vertical (axial) and horizontal (radial) components of the microburst forces. The boundary conditions at the end of each conductor span are modelled using a system of non-linear springs that simulate the stiffness

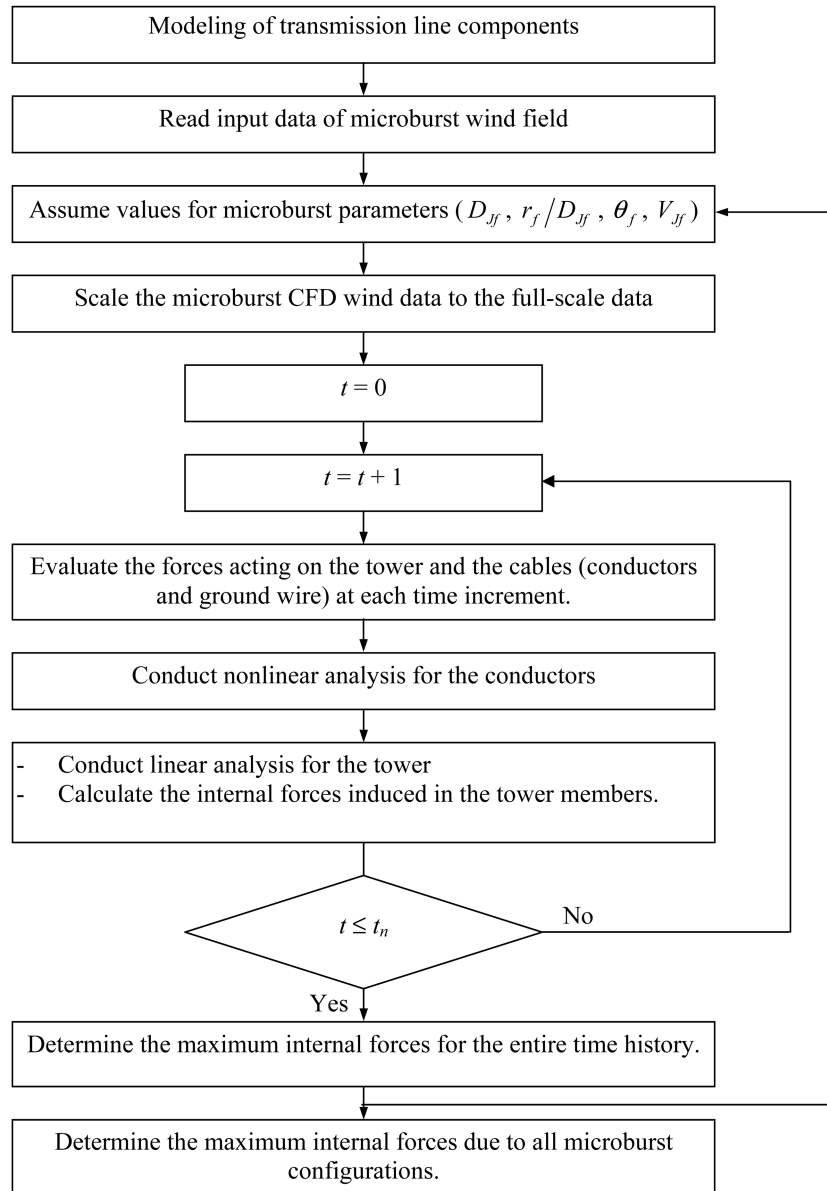


Fig. 2 Flow chart of the fluid-structure model

provided by both the tower and the insulator strings at these locations.

### 3.2. Input data of microburst wind field

A microburst event is a metrological phenomenon that is localized, unpredictable, and hard to measure by traditional recording stations. As such, the simulation of a microburst wind field is conducted numerically based on a computational fluid dynamic (CFD) model that was developed and experimentally validated by Hangan, *et al.* (2003). The CFD analysis was done for specific

values of the microburst jet diameter ( $D_{Jm} = 0.0381$  m) and jet velocity ( $V_{Jm} = 7.50$  m/s). The resulting wind field data are given as time history series (240 time steps) for the two velocity components of the microburst; the radial (horizontal) velocity component ( $V_{mRD}$ ) and the axial (vertical) velocity component ( $V_{mAX}$ ). The values of the two velocity components at a specific point in space are functions of the height of this point relative to the ground ( $Z_{ma}$ ) and its location relative to the centre of the microburst ( $r_{ma}$ ).

### 3.3. Assumed values for real microbursts parameters

The parameters that define the forces acting on a transmission tower located at the vicinity of a microburst are shown in Fig. 3. These are the jet diameter  $D_{Jf}$ , the location of the centre of the microburst relative to the centre of the tower defined by the cylindrical coordinates ( $r_f$ ,  $\theta_f$ ), and the jet velocity  $V_{Jf}$ . The current study is conducted using values of  $D_{Jf}$  varying between 250 and 2000 (m), while the ratio  $r_f/D_{Jf}$  is varied between 0.0 and 2.20 with an increment of 0.20. In view of the double symmetry, the value of the angle  $\theta_f$  is varied only between  $0^\circ$  and  $90^\circ$  with an interval of  $15^\circ$ . There is no need to vary the jet velocity  $V_{Jf}$  since it is obvious that the microburst forces will increase monotonically with an increase of  $V_{Jf}$ . A single value of  $V_{Jf} = 70$  (m/s) that represents the maximum wind speed recorded in the field during a microburst event (Savory, *et al.* 2001) is considered in the study.

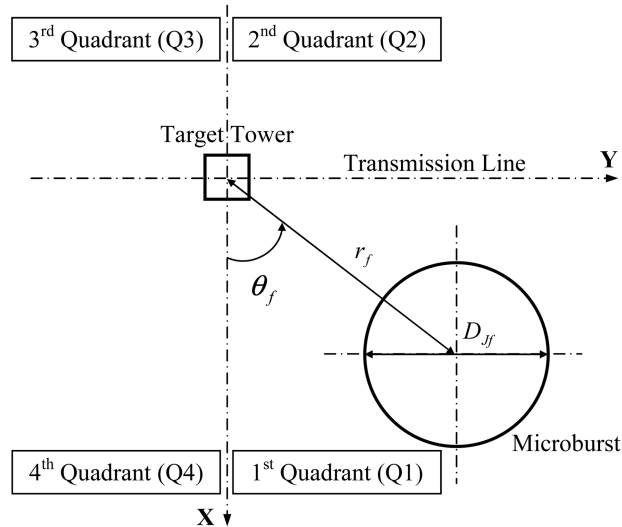


Fig. 3 Microburst characteristic parameters

### 3.4. Scaling microburst CFD data to evaluate full-scale velocity and microburst forces

The analysis starts by assuming specific values for the microburst parameters  $D_{Jf}$ ,  $r_f$  and  $\theta_f$  within the ranges defined above. The location of any point in the tower (or the conductors) relative to the centre of the microburst ( $r_{fa}$ ,  $Z_{fa}$ ,  $\theta_{fa}$ ) can be then evaluated. Based on the relative values between the prototype parameters ( $D_{Jf}$ ,  $r_{fa}$ ,  $V_{Jf}$ ,  $Z_{fa}$ ) and the model parameters ( $D_{Jm}$ ,  $r_{ma}$ ,  $V_{Jm}$ ,  $Z_{ma}$ ), a procedure to scale up the model velocity wind field data was suggested by Shehata, *et al.* (2005).

This leads to the evaluation of time history series for the radial ( $V_{RD}$ ) and axial ( $V_{AX}$ ) velocity components at any point of the structure associated with a specific microburst configuration. Knowing the velocity wind field acting on a real structure, the corresponding forces are then calculated using the ASCE No.74 guidelines (1991). As such, the time history series for the forces acting on nodal points of the tower and the conductors can be determined for any microburst configuration.

### 3.5. Parametric study to determine maximum internal forces in the tower members

It was shown by Shehata, *et al.* (2005) that the natural period of both the tower and the conductors are much lower than the natural period of the microburst loading. Consequently, the dynamic effects of both the tower and the conductors have an insignificant influence on the behaviour of the tower. As such, the analysis in the current study is carried out as quasi-static. At each time interval, the following three sets of analyses are conducted:

1. Non-linear analysis of the conductors and the ground wires under the forces associated with the radial component of the microburst. Here, the conductors and the ground wires are modelled in a horizontal plane using the 2-D curved beam model. Pre-tension axial forces applied to the cables are considered in this set of analysis.
2. Non-linear analysis of the conductors and the ground wires under the forces associated with the vertical component of the microburst. In this case, the conductors and the ground wire are modelled in a vertical plane using the same 2-D curved beam model. Pre-tension axial forces as well as the initial sagging of the cables are considered in this set of analysis.
3. Linear analysis of the tower under the combined effect of the microburst forces acting on the tower nodes and the reactions at the tower locations resulting from the previous two non-linear analyses.

The last analysis leads to the evaluation of the instantaneous values of the internal forces acting on all members of the tower. The three sets of analyses are repeated throughout the entire time history of the microburst event. For a specific microburst configuration, the maximum forces acting on each member of the tower are then evaluated. It should be noted that these maximum forces occur at different time intervals. These analyses are then repeated by varying the microburst parameters within the ranges defined earlier. The absolute maximum internal forces for each member of the tower resulting from all conducted analyses are then evaluated. For each member, the following parameters are recorded: (a) maximum axial force, (b) microburst parameters associated with this maximum force, and (c) time at which the maximum force occurs.

## 4. Determination of critical members of the tower and associated microburst parameters

Results of the conducted parametric study are used to determine the tower members that are critical to microburst loading. The microburst configurations as well as the jet velocities at which these critical members can lose their stiffness are also calculated. The compressive ( $F_C$ ) and tensile ( $F_T$ ) capacities of all members are first calculated using the ASCE standards "Design of Latticed Steel Transmission Structures (1992)". These capacities are evaluated using the member cross-sectional and material properties as specified in the design drawings of the tower. The maximum forces for all members of the tower due to microburst loading ( $F_D$ ) are evaluated from the

parametric study reported in the previous section. For each member, a factor ( $\lambda_c$ ) that relates the member maximum force to its capacity is calculated using the following relation.

$$\lambda_c = \frac{\text{member force } F_D}{\text{member capacity}(F_C \text{ or } F_T)} \tag{1}$$

Since the parametric study is conducted using an arbitrary value for the jet velocity ( $V_{Jf} = 70$  m/s), the numerical values of  $\lambda_c$  are insignificant. These values indicate in a relative sense how each member is critical to microburst loading in terms of failure. The higher the value of  $\lambda_c$ , the more critical is the member. Table 1 provides the values of  $\lambda_c$  for the ten most critical members predicted by the analysis. As shown in the table, these members are ranked according to the descending values for  $\lambda_c$ . The location of the critical members relative to the zones classification shown in Fig. 1 is given in the table. Another classification related to the structural behaviour of the region, where the critical member is located, is also provided in the table. This structural behaviour is based on a simulation of the guyed tower as a simple beam with a cantilever. The cross arm (CA) area is located above the guys location and behaves as a cantilever. The guys support (GS) area is located at the vicinity of the guys. Diagonal members in this area can be subjected to large forces associated with the guys reactions acting on the tower. Also, the chord members can be subjected to large forces associated with the negative moment acting on the top cantilever part. The main tower (MT) area is located in-between both the base support and the guys. Positive moment in this area leads to large axial forces in the chord members.

Also as shown in Table 1, the critical members are identified as either chord or diagonal members. The microburst configurations that lead to the reported values of  $\lambda_c$  are provided in the table for the ten most critical members. It can be noted that Cases 1, 3, 4, 5, 8 and 9 given in the table have all the same microburst configuration ( $\theta_f = 30^\circ$ ,  $r_f / D_{Jf} = 1.60$  and  $D_{Jf} = 1000$  (m)). As

Table 1 Input data for progressive analysis study

Case	Member No.	Zone	Location	Member Description	Failure Mechanism	Force (kN)	Capacity (kN)	$\lambda_c$	Microburst Parameters					$V_{refH}@10$ (m) Height (m/s)
									$\theta_f$	$r_f / D_{Jf}$	$D_{Jf}$ (m)	$V_{Jfc}$ (m/s)	$V_{Jfcol}$ (m/s)	
1	127	6	CA	LCCC	1	-168.0	-165.0	1.02	30°	1.60	1000	69.1	69.1	33.9
2	405	6	CA	DTS	1	-66.3	-68.5	0.97	30°	1.40	250	---	---	---
3	564	6	CA	LCCC	1	-169.0	-177.0	0.96	30°	1.60	1000	---	---	---
4	72	6	CA	UCCC	1	-70.8	-76.4	0.93	30°	1.60	1000	---	---	---
5	116	6	CA	UCCC	1	-70.2	-76.4	0.92	30°	1.60	1000	---	---	---
6	414	6	CA	DTS	2	-61.9	-68.5	0.90	0°	1.20	1000	74.2	83.5	81.4
7	396	6	GS	DTS	3	-75.1	-87.5	0.86	90°	1.20	500	75.8	81.0	84.7
8	213	6	CA	LCCC	1	-141.0	-165.0	0.85	30°	1.60	1000	---	---	---
9	411	6	GS	DTS	1	-74.3	-87.5	0.85	30°	1.60	1000	---	---	---
10	91	2	MT	CTS	3	-145.0	-173.0	0.84	90°	1.20	250	---	---	---

Notations: CA: Cross-Arms  
 GS: Guys Support  
 MT: Main Tower  
 CTS: Chord member in Tower Shaf  
 LCCC: Lower Chord member in Conductor Cross-arm  
 UCCC: Upper Chord member in Conductor Cross-arm  
 DTS: Diagonal member in Tower Shaft

such, all these cases represent one failure mechanism. This failure mechanism is denoted in Table 1 as *F1*. Case 2, associated with member # 405, has the same value for  $\theta_f = 30^\circ$  with different values for  $r_f/D_{Jf}$  and  $D_{Jf}$ . It has been shown through a progressive failure analysis that this case leads to a failure mechanism very similar to *F1*, so it is not treated as a new failure case. Also, Case 10 has the same values for  $\theta_f = 90^\circ$  and  $r_f/D_{Jf} = 1.20$  as Case 7 with different value for  $D_{Jf}$ . It has been also noticed throughout a progressive failure analysis that these two cases lead to almost the same failure mechanism and therefore are both denoted as *F3*. The third independent failure mode is associated with Case 6 that is initiated the failure of member # 414. As such, three possible failure mechanisms associated with Cases 1, 6 and 7 will be studied in the following sections of the paper.

The study then proceeds to determine the jet microburst velocity  $V_{Jf}$  at which buckling initiates at the critical members associated with the three failure mechanisms, i.e. members # 127, # 414 and # 396 shown in Fig. 4. The analyses are repeated using the three critical microburst sets of parameters ( $\theta_f$ ,  $D_{Jf}$  and  $r_f/D_{Jf}$ ) given in Table 1, while gradually increasing the jet velocity till the value of the parameter  $\lambda_c$  for the critical member reaches unity. Fig. 5 shows the variations of  $\lambda_c$  with the jet velocity for the three critical members. Results of those analyses are provided in Table 1 showing the values of  $V_{Jfc}$  for each failure mechanism. It can be seen that the first failure mechanism, that initiates at the cantilever part of the tower, occurs at the lowest value for the critical jet velocity  $V_{Jfc} = 69.1$  (m/s). This finding can be physically interpreted as follows: a microburst having a jet diameter of  $D_{Jf} = 1000$  m and a jet velocity of 69.1 m/sec is expected to initiate buckling of member # 127 located at the conductor cross-arm area of the tower if the location of the centre of the microburst relative to the centre of the tower satisfies the following relations:  $r_f/D_{Jf} = 1.60$  and  $\theta_f = 30^\circ$ .

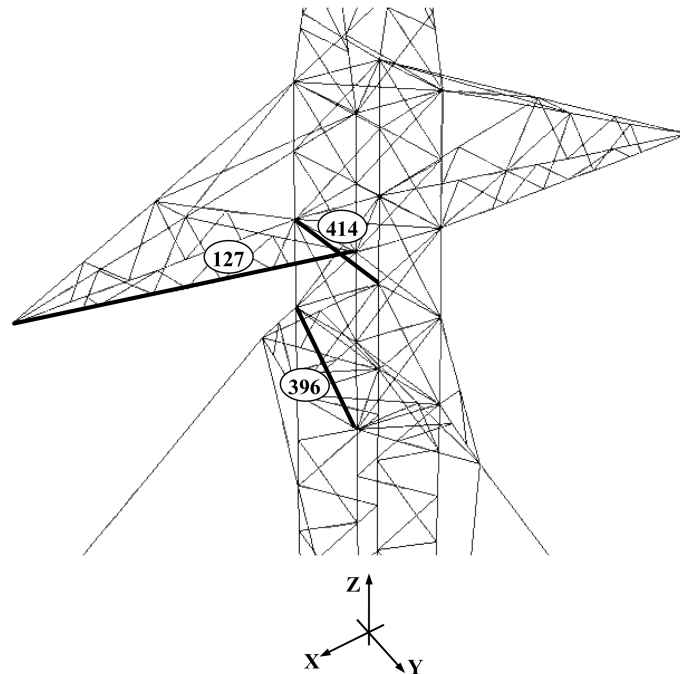


Fig. 4 Critical members of the transmission tower

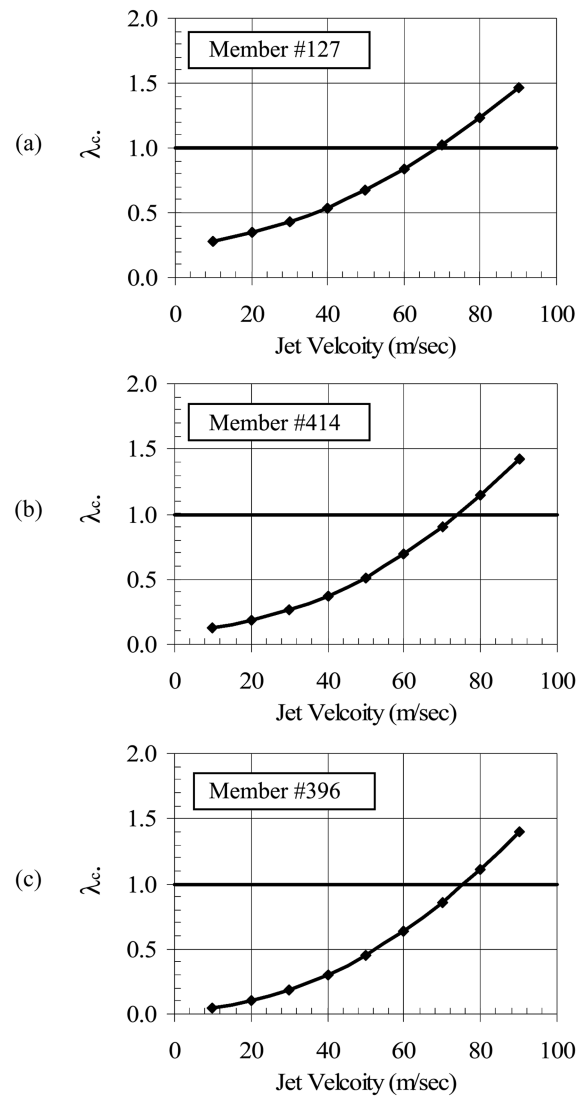


Fig. 5 Variation of the capacity factor  $\lambda_c$  with the jet velocity for Cases: (a) # 1; (b) # 6; and (c) # 7

### 5. Progressive failure analysis

The analysis of the tower proceeds to assess the progressive failure mechanism of the tower. The following steps are conducted to achieve this task.

1. Analyses are conducted for the tower using the critical microburst configurations ( $\theta_f, D_{Jf}, r_f / D_{Jf}, V_{Jfc}$ ) associated with the three distinct failure mechanisms that are provided in Table 1.
2. At each time step, the ratios  $\lambda_c$  are calculated for all members of the tower.
3. It is assumed that members that reach their compressive or tensile capacities lose their stiffness and consequently, do not contribute into the load carrying capacity of the structure. Members in tension might yield and, in this case, they would maintain a certain load carrying capacity.

However, if failure happens at the connection, the member would lose totally its load capacity. Since the connection details are not available to the authors, this conservative assumption is made in the analysis.

4. At any time increment during which the factor  $\lambda_c$  for one or more members reaches or exceeds unity, i.e.,  $\lambda_c \geq 1.0$ , iterations are conducted while assuming zero stiffness for those members. In case of numerical convergence, the analysis proceeds to the next time step. A numerical divergence indicates that the structure has lost its global stability.

## 6. Results of progressive failure analysis

A detailed description of the results of the three conducted progressive failure analyses is provided in this section. The term failure of a member is defined here as a state at which the member reaches either its compressive or its tensile capacity. In order to identify the location of a failed member, four quadrants are defined in a horizontal plane as shown in Fig. 3.

### 6.1. Failure mechanism F1 ( $\theta_f = 30^\circ$ , $r_f/D_{Jf} = 1.60$ , $D_{Jf} = 1000$ m)

The location of the microburst relative to the tower corresponding to this case is shown in Fig. 6(a). The loading associated with this microburst configuration will cause forces on the conductor spans located at one side of the tower (having positive Y-coordinates) unequal to the forces acting on the conductor spans located at the other side of the tower (having negative Y-coordinates). Consequently, the longitudinal internal axial forces developing in the two conductors adjacent to the tower will be different. As a result, a resultant force acting on the tower and parallel to the longitudinal direction of the conductor will develop. This leads to a large out-of-plane bending moment acting on the conductor cross-arm that contributes significantly into the failure of members in this portion of the tower. The progressive analysis is conducted using a jet velocity equal to the value of  $V_{Jfc} = 69.1$  (m/s) reported in Table 1. It started when buckling of member # 127 (lower chord member of the conductors cross-arm located in the first quadrant) initiated after 227.9 seconds from the beginning of the microburst event. This is followed by progressive failure of horizontal and diagonal members of the tower shaft in the cross-arm (CA) area and then progressive failure of diagonal and lower chord members of the conductor cross arm. Finally, the model predicts a total collapse of the conductors cross arm located left to the tower (having positive X-coordinates according to Fig. 6) indicating that the collapse jet velocity  $V_{Jf col}$  for this failure mechanism is the same as  $V_{Jf} = 69.1$  (m/s). This value is reported in Table 1.

Fig. 6 shows the failed members resulting from the progressive failure analysis. This failure mechanism is in agreement with the failure mode reported by Manitoba Hydro (1999) during a field survey that followed the collapse of the 19 transmission towers on September 1996. It was reported that most conductors cross-arms were damaged.

Fig. 7 shows the vertical profiles of the radial component of the microburst velocity at the centre of the tower associated with the specific microburst parameters and the jet velocity of 69.1 (m/s). An important parameter that can be used to compare the microburst and the normal velocity fields is the value of the reference wind speed at 10 meters height above the ground. The modelled tower, located in Manitoba, has been initially designed to resist normal wind loads using a reference wind speed  $V_{refN} = 34.0$  (m/sec) as specified by the report provided in Manitoba Hydro (1999). Table 1 shows the values of the microburst reference wind speed  $V_{refH}$  at 10 meters height associated with

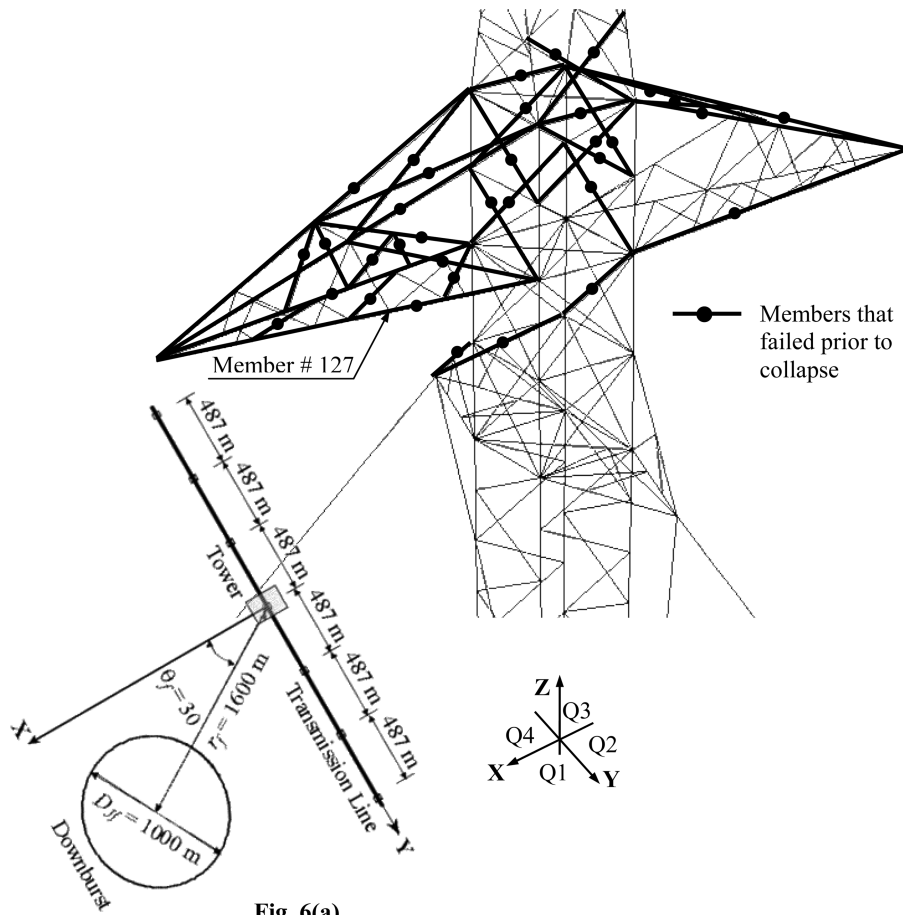


Fig. 6(a)

Fig. 6 Failure mode F1

this microburst profile. It is clear from Fig. 7 that the reference velocity under normal wind load conditions ( $V_{refN}$ ) is almost the same as the corresponding value associated with the microburst ( $V_{refH}$ ). However, the increase in velocity with height shown in the figure together with the unbalanced forces acting on adjacent spans of the conductors are the reason behind the sensitivity of the tower to this microburst configuration.

6.2. Failure mechanism F2 ( $\theta_f = 0^\circ$ ,  $r_f/D_{Jf} = 1.20$ ,  $D_{Jf} = 1000$  m)

The location of the microburst relative to the structure corresponding to this case is shown in Fig. 8(a). In this case, the conductors adjacent to both sides of the tower will be subjected to large and equal microburst loads leading to a large resultant force acting on the cantilever top part of the tower in a direction perpendicular to the conductors. This force will cause a large negative bending moment in the cantilever part of the tower as well as a large shear force in the guys area.

The progressive analysis starts by assuming a jet velocity of 74.2 (m/s), which corresponds to the value of  $V_{Jfc}$  reported in Table 1 that initiates buckling of member # 414. This is a diagonal member located in the segment of the tower bound between the conductors and the guys cross-arms

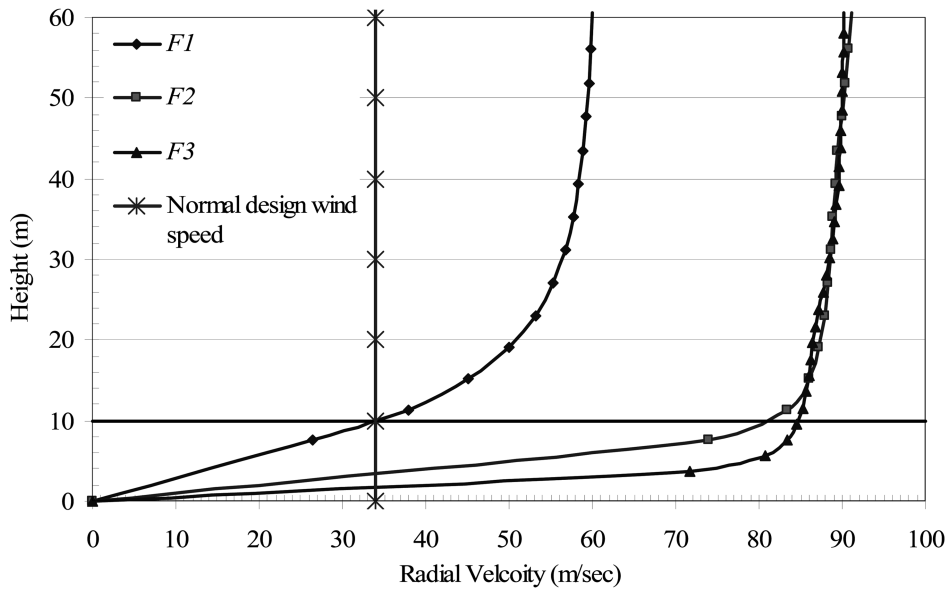


Fig. 7 Vertical profiles of microburst horizontal wind velocity associated with the three failure modes

regions. Large external shear forces in this area are responsible for the failure of this diagonal member. At the same instant, a diagonal member located at the same level as member # 414 at the opposite face of the tower has buckled. It is then noticed that no progressive failure has occurred post the buckling of these two diagonal members. The structure has enough redundancy to be able to resist the entire time history of the microburst even with the collapse of those two diagonal members. Subsequently, the progressive non-linear analysis is repeated by gradually increasing the jet velocity till the structure suffers from a state of instability. It is found that the tower loses its global stability when the jet velocity reaches a value  $V_{Jf\,col} = 83.5$  (m/s). Following the buckling of the two critical diagonal members, various members located in Zone (5) of the tower failed in a progressive manner

Fig. 8 shows the failed members resulting from the progressive failure analysis. Physically, this mode can be interpreted as an overall collapse of the tower due to the failure of its main chord members. The velocity profile associated with the jet velocity  $V_{Jf\,col} = 83.5$  (m/s) of this microburst case is provided in Fig. 7. Compared to the profile associated with the first failure mechanism, it can be seen that the reference velocity  $V_{refH}$  in this case significantly exceeds that of the first case. Also, this reference velocity exceeds well the value used in the design of the tower.

### 6.3. Failure mechanism F3 ( $\theta_f = 90^\circ$ , $r_f/D_{Jf} = 1.20$ , $D_{Jf} = 500$ m)

The location of the microburst relative to the structure correspond to this configuration is shown in Fig. 9(a). In this case, the microburst loads acting on the conductors have small magnitudes. As such, the negative moment acting on the cantilever part of the tower is negligible. This leads to an increase in the positive moment acting on the region between the guys and the bottom support of the tower. Also, large shear forces at the guys location are expected to be associated with this large positive moment. The progressive analysis is first conducted using a jet velocity of 75.8 (m/s), which leads to the initiation of buckling of a diagonal member located at the guys support (GS) area

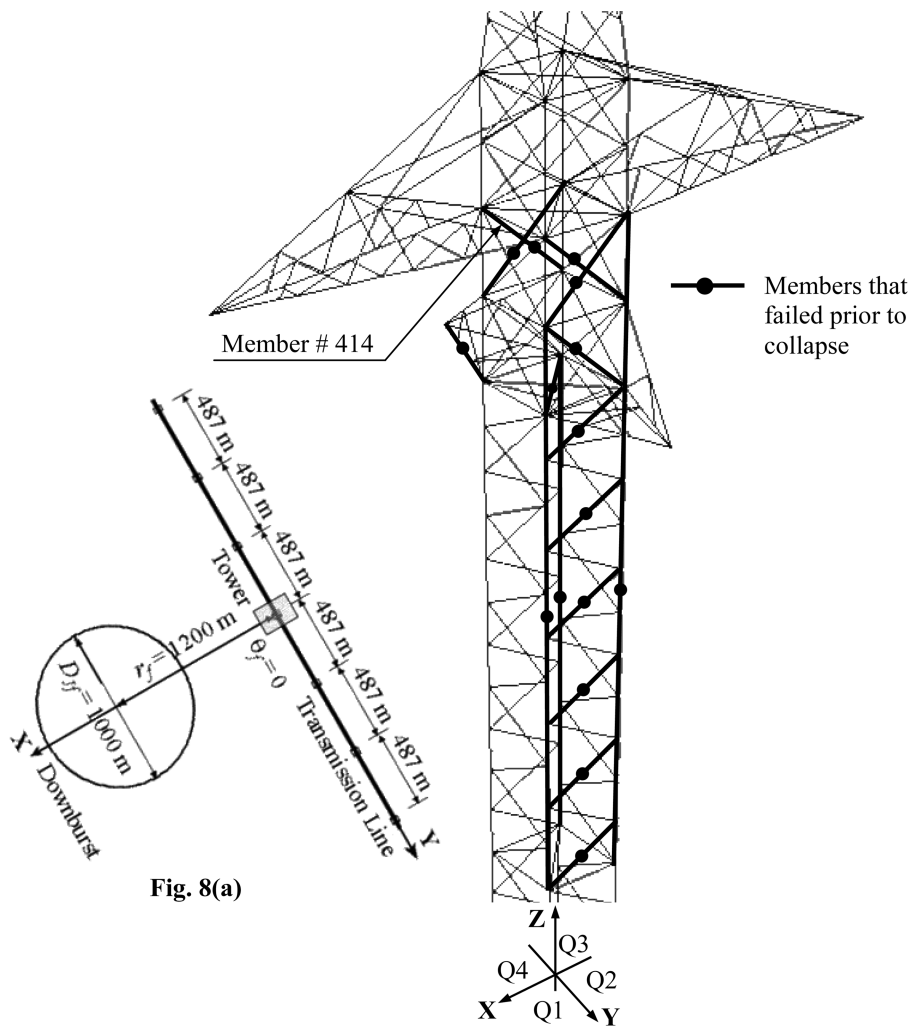


Fig. 8 Failure mode  $F2$

as a result of the above mentioned large shear force developing in this region. Similar to the previous case, at the same instant, an analog diagonal member located in the opposite face of the tower buckles. However, the structure survives the microburst loading associated with this jet velocity without suffering from global instability. The analysis has then proceeded by gradually increasing the jet velocity to determine the critical velocity  $V_{Jf\ col}$  at which the tower collapses. The analysis predicts a value of  $V_{Jf\ col} = 81.0$  (m/s). The failure of the diagonal members of the GS area is followed by failure of chord and diagonal members located in zones (2) and (3) of the tower followed by failure of members located at higher elevations.

Fig. 9 shows the failed members resulting from the progressive failure analysis. Similar to the previous case, Fig. 7 indicates that the velocity profile associated with the jet velocity  $V_{Jf\ col} = 81.0$  (m/s) and this microburst configuration has a very high value for the reference velocity  $V_{refH}$ . Physically, this failure mode can be interpreted as an overall collapse of the tower due to the failure of its main chord members.

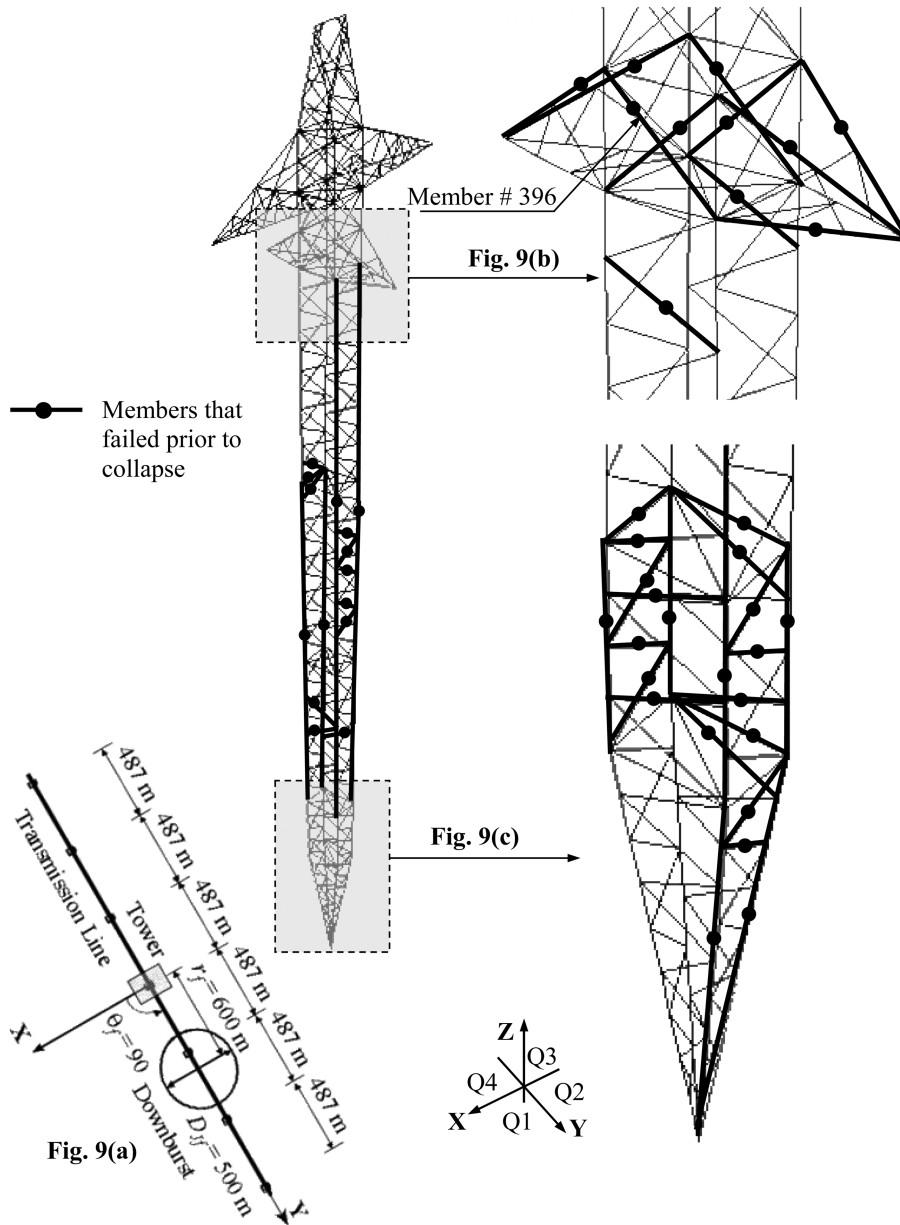


Fig. 9 Failure mode F3

### 7. Conclusions

This paper discusses the procedure of modelling and predicting the behaviour and failure modes of a transmission line structure subjected to microburst wind loads. The wind load data is based on a previously developed computational fluid dynamic (CFD) model after applying proper scaling factors. In this paper, the developed non-linear finite element model is used to predict the progressive

failure of a real tower that previously collapsed during a microburst event. The numerical model is first employed to determine the microburst parameters, such as its jet diameter and its location relative to the tower, that are most critical for the structure. A progressive failure analysis for the structure is then conducted using these microburst parameters. The most probable three scenarios of progressive failure mechanisms are discussed. The following conclusions can be drawn from the study.

1. The first failure mode can be described as a collapse of the conductors cross-arm. It is associated with a microburst having the following characteristics:  $\theta_f = 30^\circ$ ,  $r_f / D_{Jf} = 1.60$ ,  $D_{Jf} = 1000$  m, and a jet velocity  $V_{Jf\ col} = 69.1$  m/s. This microburst configuration has a reference wind velocity at 10 meters height  $V_{refH} = 33.9$  m/s, which is almost equal to the reference normal wind velocity used in designing the tower. However, the distribution of the microburst velocity along the height of the tower exceeds significantly that associated with the typical boundary layer normal wind profile. This failure mode is expected to result from large out-of-plane bending moment acting on the conductor cross-arm. This results from the unbalanced microburst loads that act on the conductor spans adjacent to the tower due to this microburst configuration.
2. The second failure mode can be described as a total collapse of the tower due to failure of its chord members. It is associated with a microburst having the following characteristics:  $\theta_f = 0^\circ$ ,  $r_f / D_{Jf} = 1.20$ ,  $D_{Jf} = 1000$  m, and a jet velocity  $V_{Jf\ col} = 83.5$  m/s. This microburst configuration has a reference wind velocity  $V_{refH} = 81.4$  m/s, which is much higher than the reference wind velocity used to design the tower in order to resist normal wind loads. This failure mode is expected to be the direct result of large negative bending moment that acts on the cantilever part of the tower due to the large balanced microburst loads acting on the adjacent spans of the conductor.
3. The third failure mode can be also described as a total collapse of the tower due to failure of its chord members. It is associated with a microburst having the following characteristics:  $\theta_f = 90^\circ$ ,  $r_f / D_{Jf} = 1.20$ ,  $D_{Jf} = 500$  m, and a jet velocity  $V_{Jf\ col} = 81.0$  m/s. This microburst configuration has a reference wind velocity  $V_{refH} = 84.7$  m/s, which exceeds significantly the reference wind velocity under normal wind loads used in the design of the tower. This microburst configuration leads to negligible forces acting on the conductors and consequently on the cantilever part of the tower. As a result, large positive bending moment occurs in the region bound by the guys and the base of the tower. It is expected that this failure mode is a direct result of this large positive bending moments values.

## Acknowledgment

The authors are obliged to the Natural Sciences and Engineering Research Council of Canada (NSERC) and Manitoba Hydro Company, Canada, for the financial and in-kind support provided to this research work. Also, the authors deeply appreciate the SHARCNET facility and staff at the University of Western Ontario, Canada. Finally, the authors acknowledge Prof. H. Hangan and Dr. J-D. Kim at the Boundary Layer Wind Tunnel Laboratory, the University of Western Ontario, Canada, for their effort in providing microburst wind data.

## Notation

- $\lambda_C$  : Capacity factor = member force / member capacity  
 $\theta_f$  : Angle between a vertical plane that contains the centres of the tower and the microburst and a vertical plane perpendicular to the transmission line

- $\theta_{fa}$  : Angle between a vertical plane that contains the point of interest and the centre of the microburst and a vertical plane perpendicular to the transmission line  
 $D_{Jf}$  : Full-scale microburst jet diameter  
 $D_{Jm}$  : Microburst jet diameter for the CFD simulation model  
 $F_C$  : Compressive capacities of tower members  
 $F_D$  : Axial internal forces in tower members due to microburst loading  
 $F_T$  : Tensile capacities of tower members  
 $r_f$  : Full-scale horizontal distance between the centres of the tower and the microburst  
 $r_{fa}$  : Full-scale horizontal distance between the point of interest and the centre of the microburst  
 $r_{ma}$  : Horizontal distance between the point of interest and the centre of the microburst for the CFD simulation model  
 $V_{AX}$  : Full-scale axial velocity component of the microburst  
 $V_{Jf}$  : Full-scale microburst jet velocity  
 $V_{Jfc}$  : Microburst jet velocity at  $\lambda_C = 1.0$  for a specific member of the tower  
 $V_{Jfcol}$  : Microburst jet velocity that leads to an overall collapse of the tower  
 $V_{Jm}$  : Microburst jet velocity for the CFD simulation model  
 $V_{mAX}$  : Axial velocity component of the microburst for the CFD simulation model  
 $V_{mRD}$  : Radial velocity component of the microburst for the CFD simulation model  
 $V_{RD}$  : Full-scale radial velocity component of the microburst  
 $V_{refH}$  : Reference wind velocity at 10 meters height under microburst wind conditions  
 $V_{refN}$  : Reference wind velocity at 10 meters height under normal wind conditions  
 $Z_{fa}$  : Full-scale height of the point of interest relative to the ground  
 $Z_{ma}$  : Height of the point of interest for the CFD simulation model relative to the ground

## References

- American Society of Civil Engineers (ASCE) (1991), "Guidelines for electrical transmission line structural loading", *ASCE Manuals and Reports on Engineering Practice*, No. 74, New York.  
 American Society of Civil Engineers (ASCE) (1992), "Design of latticed steel transmission structures", *ASCE Standard*, (ANSI/ASCE 10-90, ANSI approved, December 9, 1991), New York.  
 Gerges, R. R. and El-Damatty, A. A. (2002), "Large displacement analysis of curved beams", *Proceedings of CSCE Conference*, Montreal, QC, Canada, ST 100.  
 Hangan, H., Roberts, D., Xu, Z. and Kim, J. (2003), "Downburst simulation. Experimental and numerical challenges", *Proceedings of the 11<sup>th</sup> International Conference on Wind Engineering*, Lubbock, Texas, Electronic Version.  
 Koziey, B. and Mirza, F. (1994), "Consistent curved beam element", *Comput. Struct.*, **51**(6), 643-654.  
 McCarthy, P. and Melsness, M. (1996), "Severe weather elements associated with September 5, 1996 hydro tower failures near Grosse Isle, Manitoba, Canada", *Manitoba Environmental Service Centre, Environment Canada*, 21 pp.  
 Savory, E., Parke, G., Zeinoddini, M., Toy, N. and Disney, P. (2001), "Modelling of tornado and microburst-induced wind loading and failure of a lattice transmission tower", *Eng. Struct.*, **23**, 365-375.  
 Shehata, A. Y., El Damatty, A. A. and Savory, E. (2005), "Finite element modeling of transmission line under downburst wind loading", *Finite Element in Analysis and Design*, **42**, 71-89.  
 Transmission and Civil Design Department (1999), "Bipole 1 & 2 HVDC Transmission Line Wind Storm Failure on September 5, 1996 – Review of Emergency Response, Restoration and Design of These Lines", *Manitoba Hydro*, 98-L1/1-37010-06000, 54 pp.  
 Transmission Line Standard (1991), "Direct current guyed suspension tower type A-402-0 structural steel layout", *Engineering and Construction, Manitoba Hydro*, 1-30000-DE-25111-0002.